Pergamon

Int. J. Solids Structures Vol. 33, No. 20–22, pp. 3297–3308, 1996

0020-7683/96 $15.00 + .00

0020-7683(95)00261-8

EFFECT OF STRAIN-DEPENDENT COHESIVE ZONE MODEL ON PREDICTIONS OF CRACK GROWTH RESISTANCE

V. TVERGAARD
Department of Solid Mechanics, Technical University of Denmark, Building 404, DK-2800 Lyngby, Denmark

and

J. W. HUTCHINSON
Division of Applied Sciences, Harvard University, Cambridge, MA, U.S.A.

Abstract—Crack growth in an elastic–plastic solid is studied by a computational model, in which a cohesive zone model is used to characterize the fracture process. The separation work per unit area and the peak stress required for separation are the basic parameters in the cohesive zone model, but also an effect of plastic straining, reducing the peak stress for separation, is incorporated here. This additional effect represents acceleration of the void growth process and nucleation of more voids, resulting from intense plastic straining in the immediate vicinity of the crack tip. The analyses are carried out for conditions of small-scale yielding under plane strain, with the mode I stress intensity factors specified at the loading parameter. Also the effect of a T-stress on crack growth resistance is investigated. Copyright © 1996 Elsevier Science Ltd.

1. INTRODUCTION

It is well known that dissipation in the plastic zone surrounding a crack tip makes a major contribution to the macroscopic work of fracture of ductile materials. For metals and metal–ceramic interfaces which fracture by an atomic separation mechanism, the atomistic work of fracture is typically on the order of $\Gamma_0 = 1\ \mathrm{J\ m^{-2}}$, while it is not uncommon for the macroscopic work of fracture Γ_{ss} needed to propagate a crack under steady-state conditions to be as much as $100\ \mathrm{J\ m^{-2}}$ or even $1000\ \mathrm{J\ m^{-2}}$. For the materials of concern in this paper (metals failing by the mechanism of void nucleation, growth and coalescence) the work of the fracture process is not always easy to identify. When separation takes place as a plane of localized deformation with coalescing voids strung out ahead of the crack tip, Γ_0 is the work per unit area expended in growing and coalescing the voids in this plane. It is approximately $\Gamma_0 = \sigma_Y D/2$, where σ_Y is the tensile yield stress of the metal and D is the average void spacing (Tvergaard and Hutchinson, 1992). For structural metals, Γ_0 is typically in the range from 10^2 to $10^4\ \mathrm{J\ m^{-2}}$. The macroscopic work of fracture for steady-state crack advance in structural metals fracturing by this mechanism is often many times Γ_0, amplified by plastic dissipation in a zone which extends on either side of the fracture plane over distances which are large compared to the size of the fracture process zone.

Tvergaard and Hutchinson (1992) have studied the role of plastic deformation in amplifying crack growth resistance using a cohesive zone model. They account for the interaction of the fracture process with the surrounding plastic zone by replacing the fracture process by a traction–separation relation applied on the plane of the crack which, in turn, is embedded within an elastic–plastic continuum. The most important parameters specifying the traction–separation law (see Fig. 1) are the separation work per unit area Γ_0 and the peak stress required for separation $\hat{\sigma}$. Under small scale yielding, the steady-state macroscopic work of fracture predicted by the model has the form

$$\Gamma_{ss} = \Gamma_0 F\left(\frac{\hat{\sigma}}{\sigma_Y}, \quad N\right), \tag{1}$$

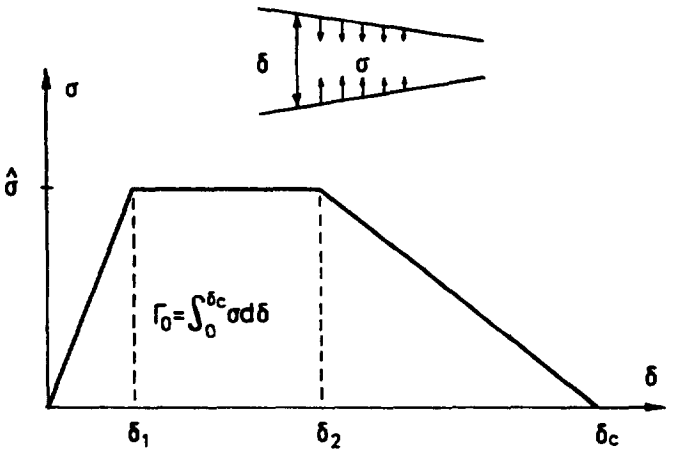

Fig. 1. Traction–separation relation for fracture process.

where the amplification factor F depends primarily on the dimensionless parameters shown with N as the strain hardening exponent. Plots of F for three values of N are shown in Fig. 2a using values taken from Tvergaard and Hutchinson (1992). Included in Fig. 2b are plots reproduced from the same reference of the normalized peak separation stress $\hat{\sigma}/\sigma_Y$, as a function of the volume fraction f_0 of the initial void population in the material. The peak stress was computed using the Gurson model (1977) under the assumption that the void-containing material elements in the separation plane undergo uniaxial straining.

Consider first the implications of the two plots in Fig. 2 for an elastic–perfectly plastic material with $N = 0$. Essentially no amplification of the steady-state toughness Γ_{ss} occurs if $\hat{\sigma}/\sigma_Y < 2$, because separation occurs so readily that a substantial plastic zone does not form. At the other limit, for peak stresses $\hat{\sigma}$ above $2.97\sigma_Y$ when $N = 0$, amplification becomes unbounded according to the model. The maximum stress achievable ahead of a crack tip in an elastic–perfectly plastic solid is $2.97\sigma_Y$, and thus separation cannot occur if $\hat{\sigma}$ exceeds this level. As it stands, the model predicts that the crack tip would simply blunt without advancing if $\hat{\sigma}$ exceeds $2.97\sigma_Y$. Now turn to the trend in $\hat{\sigma}$ as a function of initial void volume fraction f_0 for $N = 0$ in Fig. 2b. The trends in the normalized steady-state toughness with the dependence on $\hat{\sigma}$ re-expressed in terms of f_0 are displayed in Fig. 3. For materials with no strain hardening and f_0 less than about 0.01, $\hat{\sigma}$ exceeds $2.97\sigma_Y$ and therefore cracks would not propagate in this material. However, if more voids nucleate as plastic straining occurs, f_0 and the corresponding value of $\hat{\sigma}$ decay, so that the relevant value of $\hat{\sigma}/\sigma_Y$ may fall below $2.97\sigma_Y$, giving rise to crack propagation. The transition value of peak stress $\hat{\sigma}$ for a hardening material with $N = 0.1$ is about $3.9\sigma_Y$ corresponding to f_0 less than about 0.007, as can be seen in Fig. 3. For $N = 0.2$, the transition values from Fig. 2 are less well determined but $\hat{\sigma}$ can be seen to lie between 5 and 6 times σ_Y. This corresponds to a value of f_0 of about 0.003.

The trends outlined above are accompanied by a transition in important details of the fracture process mechanism. For values of f_0 above this transition the fracture process involves multiple voids growing and coalescing ahead of the tip. This is the *multiple void interaction regime* indicated in Fig. 3, for which the cohesive zone model described above is intended. For values of f_0 below the transition the process is primarily the interaction of the crack tip and the void nearest to it. The cohesive zone model described above is not adequate as it stands in the *void by void crack advance regime*. The intense deformation very near the tip amplifies the growth of the void at the tip above what it would experience in the separation plane further away from the tip. This same deformation may also bring about the nucleation of new voids, effectively lowering the peak separation stress. One possible approach to predicting crack growth in the regime of void by void advance is to incorporate material elements containing individual voids in the crack model. Void nucleation in the elements can also be included. This is the approach taken by a number of researchers including Needleman and Tvergaard (1987), Rousselier (1987), Brocks *et al.*

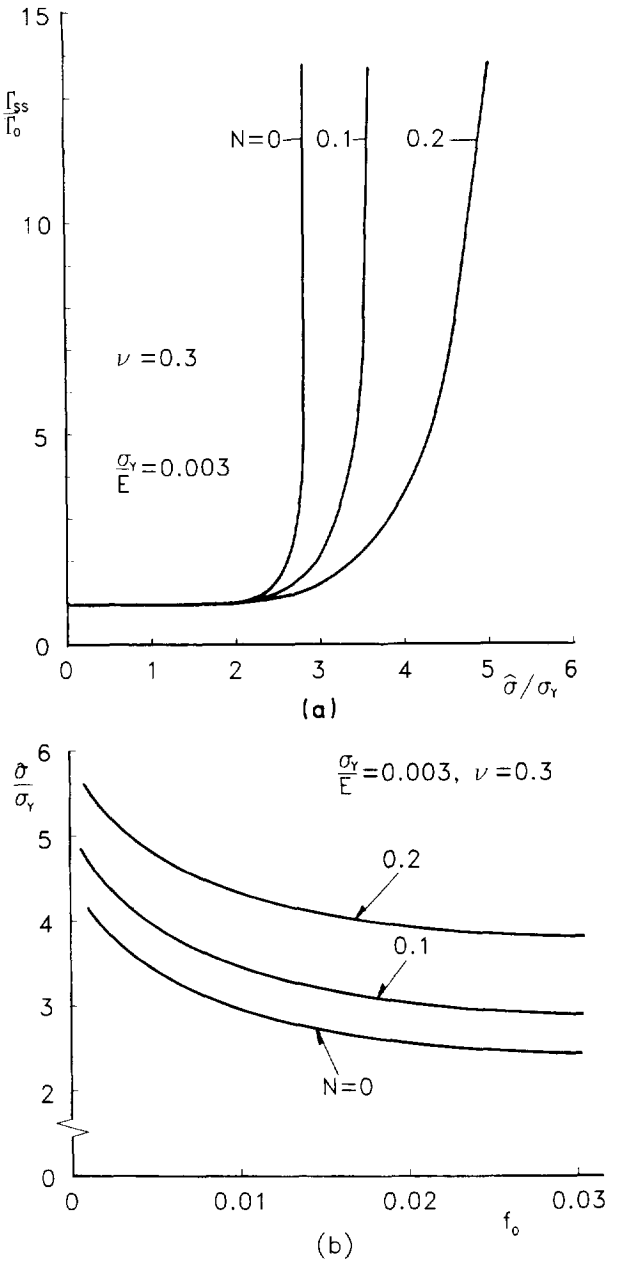

Fig. 2. (a) Steady-state macroscopic work of fracture vs peak separation stress. (b) Peak stress vs initial void volume fraction, in a uniaxial strain state for no nucleation.

(1994) and Xia *et al.* (1995). In these models the spacing between the voids is an essential parameter (as will be discussed in the final section of the paper) and crack growth is computed as a process of discrete incremental advances of the tip from void to void. An alternative approach will be pursued here wherein the cohesive zone model introduced in the earlier work (Tvergaard and Hutchinson, 1992) will be extended to model the effect of the intense near-tip plastic deformation on the traction–separation relation. The primary modification is inclusion of an effect of crack tip plastic straining on the peak separation stress $\hat{\sigma}$, which is assumed to arise from either strain-induced void nucleation or accelerated void growth. This extension of the model is qualitative in the sense that the modification is not directly related to void growth or nucleation mechanics. Nevertheless, the modification mimics behaviour expected in the regime of void by void growth, and therefore the model expands the scope of the earlier model and reveals the limits of its validity.

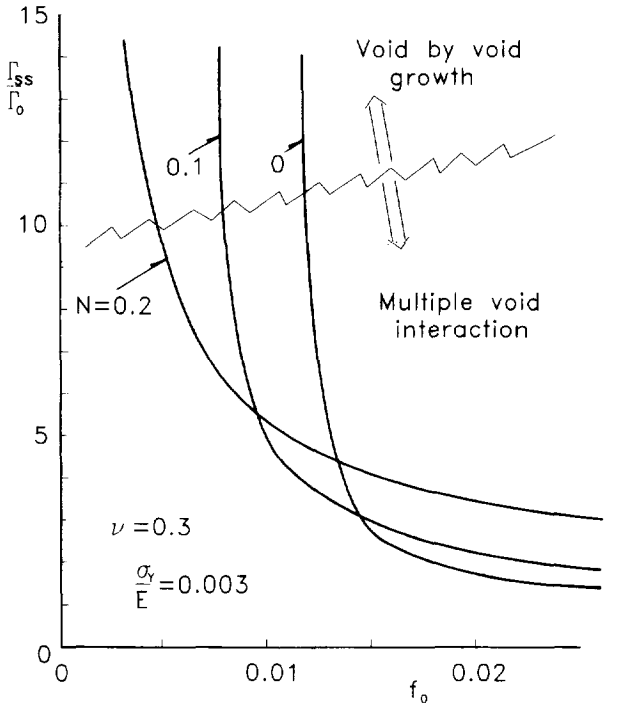

Fig. 3. Steady-state macroscopic work of fracture vs initial void volume fraction.

2. PROBLEM FORMULATION AND NUMERICAL PROCEDURE

The elastic–plastic solid to be analysed has an initial yield stress σ_Y and a uniaxial true stress–logarithmic strain curve specified by

$$\varepsilon = \begin{cases} \sigma/E, & \text{for } \sigma \leqslant \sigma_Y \\ (\sigma_Y/E)(\sigma/\sigma_Y)^{1/N}, & \text{for } \sigma \geqslant \sigma_Y. \end{cases} \tag{2}$$

This behaviour is generalized to multiaxial stress states assuming isotropic hardening and using the Mises yield surface, so that the continuum behaviour of the solid is characterized by the set of parameters E, ν, σ_Y and N.

Finite strains are accounted for in the analysis (using a convected coordinate, Lagrangian formulation of the field equations) in which g_{ij} and G_{ij} are metric tensors in the reference configuration and the current configuration, respectively, with determinants g and G, and $\eta_{ij} = 1/2(G_{ij}-g_{ij})$ is the Lagrangian strain tensor. The contravariant components τ^{ij} of the Kirchhoff stress tensor on the current base vectors are related to the components of the Cauchy stress tensor σ^{ij} by $\tau^{ij} = \sqrt{G/g}\,\sigma^{ij}$. Then, in the finite-strain generalization of J_2-flow theory discussed by Hutchinson (1973), the incremental stress–strain relationship is of the form $\dot{\tau}^{ij} = L^{ijkl}\dot{\eta}_{kl}$, with the tensor of instantaneous moduli given by

$$L^{ijkl} = \frac{E}{1+\nu}\left[\tfrac{1}{2}(G^{ik}G^{jl}+G^{il}G^{jk}) + \frac{\nu}{1-2\nu}G^{ij}G^{kl} - \beta\frac{3}{2}\frac{E/E_t-1}{E/E_t-(1-2\nu)/3}\frac{s^{ij}s^{kl}}{\sigma_e^2}\right]$$
$$-\tfrac{1}{2}(G^{ik}\tau^{jl}+G^{jk}\tau^{il}+G^{il}\tau^{jk}+G^{jl}\tau^{ik}). \tag{3}$$

Here, the effective Mises stress is $\sigma_e = (3s_{ij}s^{ij}/2)^{1/2}$, for $s^{ij} = \tau^{ij}-G^{ij}\tau^k_k/3$, and the value of β is 1 or 0 for plastic yielding or elastic unloading, respectively. Furthermore, E_t is the slope of the true stress vs natural strain curve at the stress level σ_e.

The traction–separation relation used by Tvergaard and Hutchinson (1992, 1994) to model the fracture process is shown in Fig. 1. This separation law is fully specified by the work of separation Γ_0, the peak stress $\hat{\sigma}$ and the shape parameters δ_1/δ_c and δ_2/δ_c. According

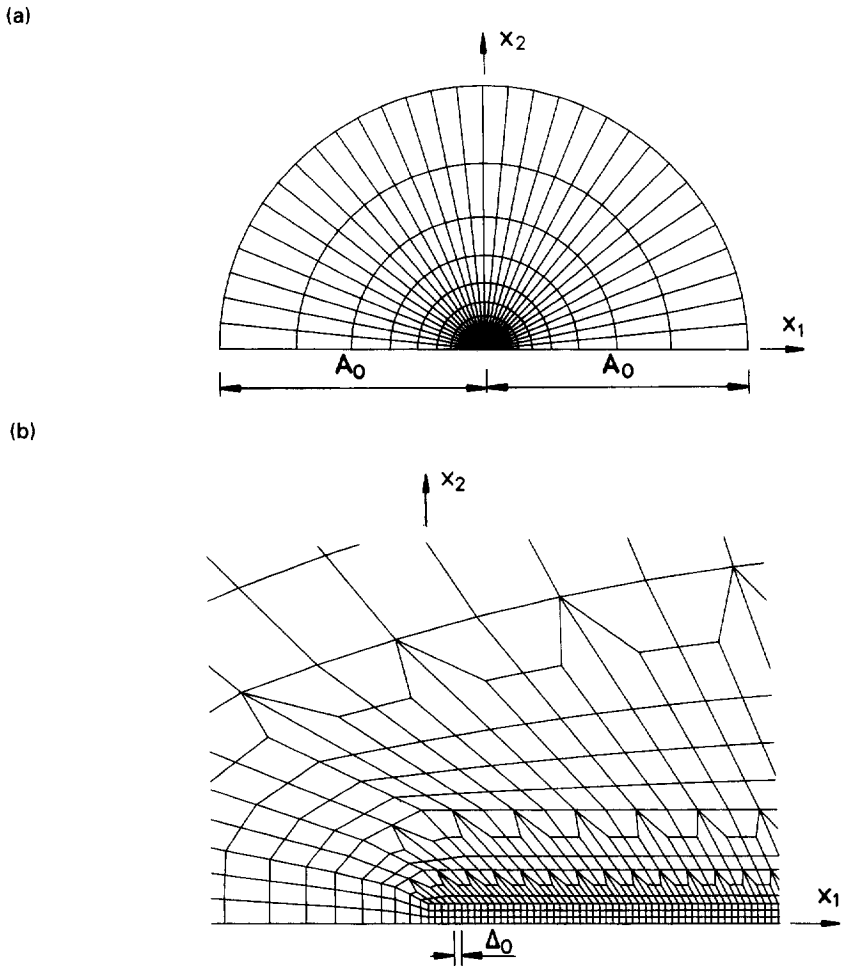

Fig. 4. Example of a finite element mesh. (a) Full mesh. (b) Refined mesh along the crack line.

to this model, failure initiates when the true normal stress ahead of the crack reaches the value $\hat{\sigma}$, and no crack growth is predicted at all if the stress level $\hat{\sigma}$ is not reached. A modification of a cohesive zone model to represent a plastic strain controlled failure mechanism has been employed by Tvergaard (1992, 1994) in studies of ductile particle debonding during crack bridging in ceramics. With this modification the peak stress $\hat{\sigma}$ in the traction–separation relation of Fig. 1 is gradually reduced when the effective plastic strain ε_e^P along the crack path has exceeded a critical value ε_c:

$$\hat{\sigma} = \begin{cases} \hat{\sigma}_0, & \text{for} \quad \varepsilon_e^P \leqslant \varepsilon_c \\ \hat{\sigma}_0 - \Delta\hat{\sigma}(\varepsilon_e^P - \varepsilon_c)/\Delta\varepsilon, & \text{for} \quad \varepsilon_c < \varepsilon_e^P < \varepsilon_c + \Delta\varepsilon. \\ \hat{\sigma} - \Delta\hat{\sigma}, & \text{for} \quad \varepsilon_e^P \geqslant \varepsilon_c + \Delta\varepsilon \end{cases} \tag{4}$$

Thus, with eqn (4) the cohesive zone model accounts for a reduction of the material strength, which could result from plastic strain controlled nucleation of voids or from accelerated void growth near the crack tip.

The crack growth analyses are carried out for conditions of small-scale yielding. Due to symmetry about the crack plane only half of the solid needs to be analysed, and the numerical computations are carried out for a semicircular region with initial radius A_0, as shown in Fig. 4. The x^1-axis is in the crack plane and the initial crack-tip is located at $x^1 = x^2 = 0$. The traction–separation relation used to model the fracture process [see Fig. 1 and eqn (4)] is specified everywhere on the boundary $x^1 > 0$ and $x^2 = 0$ of the

region analysed, while zero tractions are specified for $x^1 \leqslant 0$ and $x^2 = 0$. On the outer semi-circular boundary, displacements are prescribed in accordance with the small strain linear elastic mode I solution, for which the in-plane stress components near the crack-tip are of the form

$$\sigma_{\alpha\beta} = \frac{K}{\sqrt{2\pi r}} f_{\alpha\beta}(\theta) + T\delta_{1\alpha}\delta_{1\beta}, \tag{5}$$

where (r, θ) are polar coordinates and δ_{ij} is Kronecker's delta. The T-stress is taken to be zero in most of the present analyses, but when T is non-zero the T-stress is applied first, together with the corresponding transverse stress $\sigma_{33} = \nu T$ under plane strain conditions. Subsequently, additional displacements are specified on the outer boundary according to the singular K-field solution, by incrementally increasing the amplitude K. At some stages of the deformation the value of the J-integral is calculated on a number of contours around the crack-tip to check agreement with the prescribed amplitude K of the edge displacements, and very good agreement is found in all the present computations.

Some computations have been carried out using the mesh also employed by Tvergaard and Hutchinson (1992, 1994), while other computations make use of the slightly different mesh shown in Fig. 4. In either case, a uniform mesh region with initial length B_0 in front of the initial crack-tip is used to model crack growth. The solutions are obtained by a linear incremental method using a finite element approximation of the displacement fields in the incremental version of the principle of virtual work. The elements used are quadrilaterals each built-up of four triangular linear-displacement elements. In the uniform mesh region in front of the initial crack-tip the length of one square element is denoted as Δ_0. The present computations are carried out with $\delta_c = 0.1\Delta_0$, $\delta_1/\delta_c = 0.15$ and $\delta_2/\delta_c = 0.5$. The meshes used have $B_0 = 60\Delta_0$, or in a few cases $B_0 = 180\Delta_0$. In most of the computations the external radius of the region analysed is $A_0 = 40{,}000\Delta_0$, but $A_0 = 80{,}000\Delta_0$ has been used in a few cases. A special Rayleigh–Ritz finite element method is employed to control nodal displacements within the fracture process zone (see also Tvergaard, 1990b). This is necessary when K has reached the steady-state value while the crack still grows. The value of the effective plastic strain ε_e^P in eqn (4) is calculated as the average over the quadrilateral element adjacent to the point considered in the debonding region.

Two reference quantities, K_0 and R_0, are used for the presentation of results

$$K_0 = [E\Gamma_0/(1-\nu^2)]^{1/2}, \tag{6}$$

$$R_0 = \frac{1}{3\pi}\left(\frac{K_0}{\sigma_Y}\right)^2 = \frac{1}{3\pi}\frac{E\Gamma_0}{(1-\nu^2)\sigma_Y^2}. \tag{7}$$

Here, K_0 represents the mode I stress intensity factor needed to advance the crack when plastic dissipation is negligible, i.e. the value needed to supply just the work of the fracture process Γ_0, when the modification in eqn (4) is not active. The expression for Γ_0 is

$$\Gamma_0 = \int_0^{\delta_c} \sigma \, d\delta = \tfrac{1}{2}\hat{\sigma}_0[\delta_c + \delta_2 - \delta_1]. \tag{8}$$

The reference length R_0 scales with the size of the plastic zone when $K \simeq K_0$.

3. RESULTS

The elastic–plastic material to be analysed here is taken to be characterized by the parameter values $N = 0.1$ and $\sigma_Y/E = 0.003$ in (2), and the value of Poisson's ratio is $\nu = 0.3$. For the traction–separation relation the two parameters $\hat{\sigma}_0$ and Γ_0 (or K_0) will appear directly in the figures presenting the results, and additional parameters are those

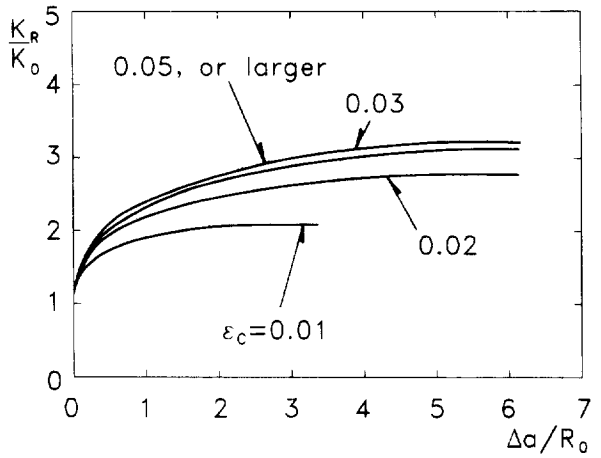

Fig. 5. Crack growth resistance curves for $\hat{\sigma}_0/\sigma_Y = 3.6$ and $T/\sigma_Y = 0$.

defining shape, $\delta_1/\delta_c = 0.15$, $\delta_2/\delta_c = 0.5$, and the maximum separation to mesh size ratio, $\delta_c/\Delta_0 = 0.1$. The same set of parameters has been used in previous analyses of the effect of plasticity on crack growth resistance (Tvergaard and Hutchinson, 1992, 1994).

Figure 5 shows crack growth resistance curves computed for $\hat{\sigma}_0/\sigma_Y = 3.6$, with zero T-stress. For the case where ε_e^P has no influence on debonding (ε_c large in eqn (4)) this was also analysed by Tvergaard and Hutchinson (1992) to determine the relative value of the steady-state toughness K_{ss}/K_0. In Fig. 5 the effect of a plastic strain-controlled failure mechanism eqn (4) is considered, taking $\hat{\sigma}_0/\sigma_Y = 3.6$, $(\hat{\sigma}_0 - \Delta\sigma)/\sigma_Y = 0.1$ and $\Delta\varepsilon = 0.05$. It is seen that for $\varepsilon_c = 0.01$ the steady-state value K_{ss}/K_0 is much reduced, and the peak toughness is reached at about half the crack growth, Δa. For $\varepsilon_c = 0.03$ the values of K_R/K_0 at a given value of $\Delta a/R_0$ are only slightly reduced, and for $\varepsilon_c = 0.05$ (or larger) the modification of the traction–separation law to account for plastic straining has no effect. It is noted in relation to Figs 2 and 3 that Γ_R/Γ_0 is simply $(K_R/K_0)^2$.

In the analysis of Fig. 6 all parameter values are the same as those used in the previous figure, apart from $\hat{\sigma}_0/\sigma_Y = 4.0$. For this higher value of the peak stress a steady-state toughness was not reached in the range analysed by Tvergaard and Hutchinson (1992), and no steady-state is reached in Fig. 6 in the range considered, apart from the case of the lowest critical strain for the onset of plastic strain controlled failure, $\varepsilon_c = 0.01$. For increasing values of ε_c the levels of K_R/K_0 increase significantly, so that for $\varepsilon_c = 0.07$ the highest

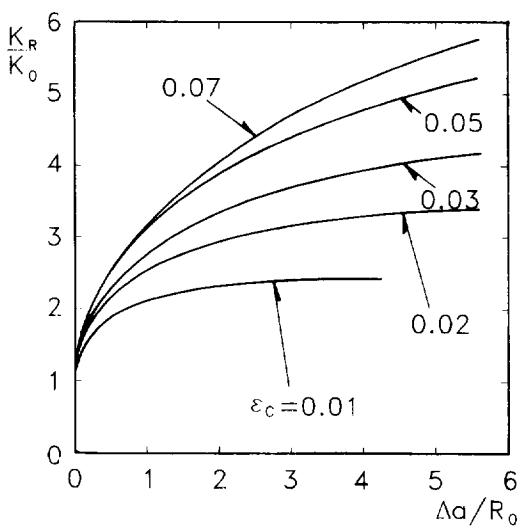

Fig. 6. Crack growth resistance curves for $\hat{\sigma}_0/\sigma_Y = 4.0$ and $T/\sigma_Y = 0$.

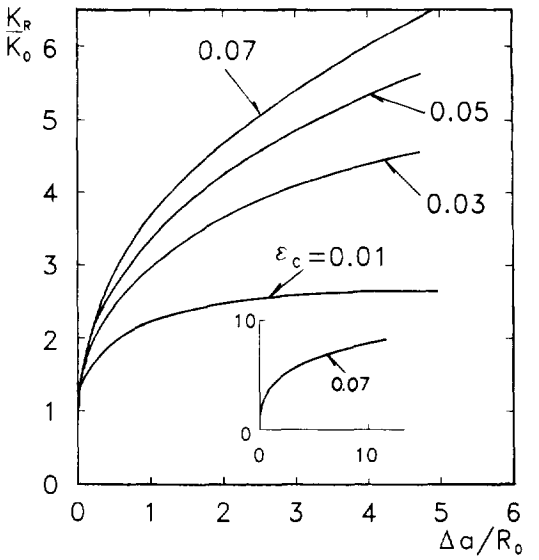

Fig. 7. Crack growth resistance curves for $\hat{\sigma}_0/\sigma_Y = 4.4$ and $T/\sigma_Y = 0$.

value of K_R/K_0 shown is 5.7, indicating that a much higher steady-state toughness may be reached at somewhat larger values of $\Delta a/R_0$.

Similar curves for an even higher value of the peak stress in the process region, $\hat{\sigma}_0/\sigma_Y = 4.4$, are shown in Fig. 7. Also here a steady state is reached for $\varepsilon_c = 0.01$, but at a larger value of $\Delta a/R_0$ than that found in Fig. 6. For the highest critical strain value considered ($\varepsilon_c = 0.07$) a value of K_R/K_0 as high as 6.5 is reached at $\Delta a/R_0 = 4.9$. The insert in Fig. 7 shows this computation continued to $\Delta a/R_0 = 12$, where $K_R/K_0 \simeq 8.25$, and here the positive slope at the end of the curve suggests that reaching a steady state would require continuation of the crack growth computation to a significantly larger value of $\Delta a/R_0$. The insert in Fig. 7 is obtained by using $B_0 = 180\Delta_0$, and further continuation would require an even larger uniform mesh region in front of the initial crack tip. However, the effect of the plastic strain controlled failure mechanism (4) on the predicted resistance curves is sufficiently well illustrated by the initial parts of the curves shown in Figs 6 and 7. As discussed in the Introduction, the fully stress-controlled debonding model cannot predict crack growth for $N = 0$ if $\hat{\sigma}/\sigma_Y > 2.97$, and for $N = 0.1$ the value of $\hat{\sigma}/\sigma_Y$ should be smaller than about 3.9. But the present studies with the plastic strain controlled failure mechanism (4) show much crack growth even for $\hat{\sigma}_0/\sigma_Y = 4.4$.

The possibility of using the crack growth model with stress-controlled debonding to present resistance curves for very tough pressure vessel steels was discussed by Tvergaard and Hutchinson (1994), in terms of the non-dimensional *tearing modulus* introduced by Paris *et al.* (1979). It was concluded that the initial slope of curves such as that for $\varepsilon_c = 0.05$ in Fig. 5 can be interpreted as a tearing modulus of no more than about 100, which is only about half the values of the tearing modulus for the nuclear pressure vessel steel A533B or the ASTM 719 grade A steel. Now, by comparing the initial parts of the resistance curves in Figs 5–7, it is seen that the initial slope does increase when a higher value of $\hat{\sigma}_0/\sigma_Y$ is used together with the strain-controlled failure mechanism. Thus, it appears that the crack growth model studied in the present paper will be able to better model the behaviour of the toughest materials.

Comparison of the resistance curves in Figs 6 and 7 shows that rather similar curves can be obtained by different combinations of the parameter values $\hat{\sigma}_0/\sigma_Y$ and ε_c. Thus, in the range shown, the curve for $\hat{\sigma}_0/\sigma_Y = 4.0$ and $\varepsilon_c = 0.07$ in Fig. 6 is seen (by interpolation in Fig. 7) to be rather close to a curve for $\hat{\sigma}_0/\sigma_Y = 4.4$ and $\varepsilon_c \simeq 0.045$. Similarly, the curve for $\hat{\sigma}_0/\sigma_Y = 4.0$ and $\varepsilon_c = 0.03$ would be rather close to a curve for $\hat{\sigma}_0/\sigma_Y = 4.4$ and $\varepsilon_c \simeq 0.025$.

It has been noted above that crack growth models based on porous ductile material descriptions are strongly mesh-dependent (e.g. see Needleman and Tvergaard, 1994). Thus, for the dilatant plasticity models the mesh size is actually used to represent the void spacing

ahead of the crack. Also the present cohesive zone representation of the process region leads to mesh sensitivity, when a plastic strain-controlled failure mechanism is incorporated in terms of (4). However, in the present model two length scales are specified for the process region, i.e. the maximum separation δ_c in the cohesive zone and the mesh size Δ_0 in the process region, and it turns out that the mesh sensitivity depends only on the value of the ratio δ_c/Δ_0, which is 0.1 in Figs 5–7. In addition, R_0 in eqn (7) defines a length, which scales with δ_c for fixed values of $\hat{\sigma}_0/\sigma_Y$, σ_Y/E and ν. The curve for $\varepsilon_c = 0.03$ and $\hat{\sigma}_0/\sigma_Y = 4.0$ in Fig. 6 has been recomputed using a mesh twice as fine, without changing the value of δ_c, and this resulted in a higher resistance curve similar to that for $\varepsilon_c = 0.07$ in Fig. 6, with a higher initial slope. On the other hand, a computation using half the value of both Δ_0 and δ_c gives a resistance curve identical to that in Fig. 6. Thus, comparing this to the resistance curves shown in Figs 5–7, the mesh dependence is such that a value of δ_c/Δ_0 larger than 0.1 will tend to give higher resistance curves than those shown in the figures, and a value smaller than 0.1 will tend to give lower curves, for fixed values of all other parameters. When Xia *et al.* (1994) use a modified Gurson model (Tvergaard, 1990a) with a fixed set of material parameters to compare resistance curves for different specimen geometries, they must use the same mesh size in the crack growth region in all computations. The same will be true for the crack growth model studied in the present paper, since the material parameters to be kept fixed include δ_c.

The cohesive zone based crack growth model describing a fully stress-dependent failure criterion has been used by Tvergaard and Hutchinson (1994) to study the effect of a T-stress. This study is extended here to consider the effect of a plastic strain-controlled failure mechanism, as represented by (4). As described in connection with eqn (5) the T-stress is applied first in these small scale yielding analyses, and subsequently the amplitude K of the singular mode I solution is increased incrementally. Only T-stress levels below the yield limit for uniaxial plane strain tension or compression are applied, so that the onset of yielding follows K, and so that the radius A_0 of the region analysed is much larger than the final plastic zone size in all cases.

Figure 8 shows resistance curves computed for $\hat{\sigma}/\sigma_Y = 4.0$ and $\varepsilon_c = 0.03$, for different values of T. Apart from T all parameter values and mesh sizes are identical to those considered in Fig. 6, and thus the curve for $T = 0$ in Fig. 8 is identical to that for $\varepsilon_c = 0.03$ in Fig. 6. As expected, based on the results of Tvergaard and Hutchinson (1994), the curve for $T/\sigma_Y = 0.5$ differs only little from that corresponding to zero T-stress, whereas the resistance curves for negative T-stress values show significantly increased toughness. At $\Delta a/R_0 = 5.5$ the value K_R/K_0 is a great deal higher for $T/\sigma_Y = -1$ than for $T = 0$ or $T/\sigma_Y = 0.5$. The insert in Fig. 8 shows the curves for $T/\sigma_Y = 0$ and for $T/\sigma_Y = -0.8$

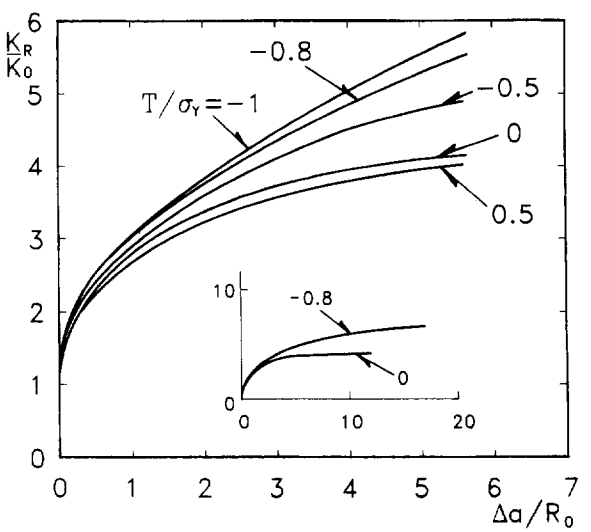

Fig. 8. Crack growth resistance curves for $\hat{\sigma}_0/\sigma_Y = 4.0$ and $\varepsilon_c = 0.03$.

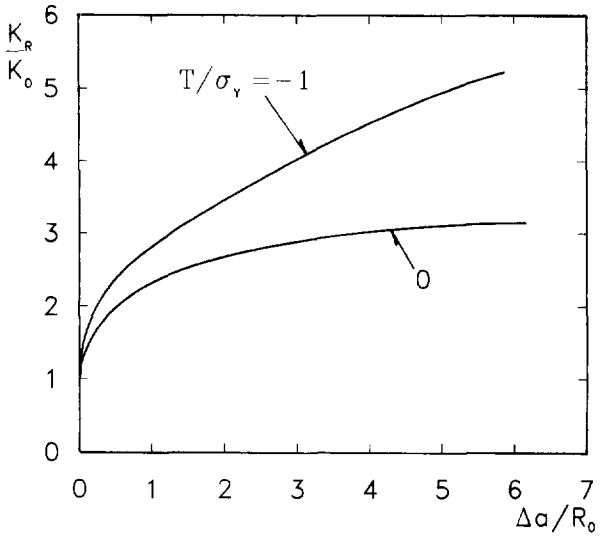

Fig. 9. Crack growth resistance curves for $\hat{\sigma}_0/\sigma_Y = 3.6$ and $\varepsilon_c = 0.03$.

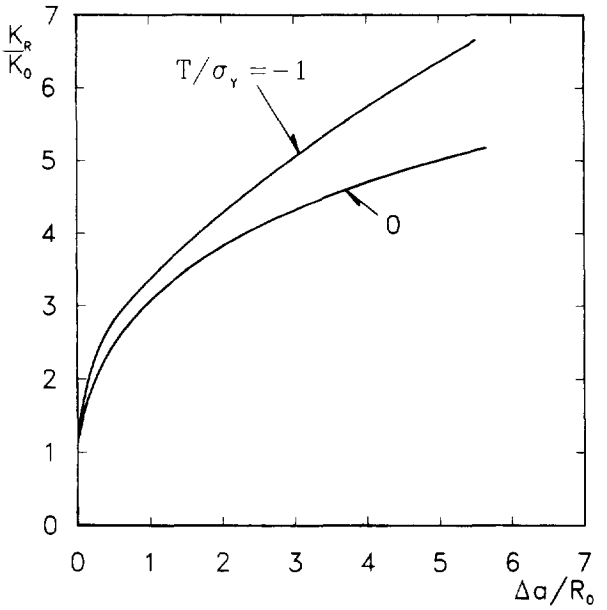

Fig. 10. Crack growth resistance curves for $\hat{\sigma}_0/\sigma_Y = 4.0$ and $\varepsilon_c = 0.05$.

continued to values of $\Delta a/R_0$ as large as 17, and it is seen that the first curve reaches a steady-state at $K^{ss}/K_0 = 4.30$, whereas the latter curve keeps growing beyond the value $K_R/K_0 = 6.73$ reached in the insert.

In Fig. 9 similar results are shown for a lower value of the debonding peak stress, $\hat{\sigma}_0/\sigma_Y = 3.6$, but still for $\varepsilon_c = 0.03$. Thus, the resistance curve for $T = 0$ is identical to that for $\varepsilon_c = 0.03$ in Fig. 5. In this case the effect of negative T-stress is stronger than that found in Fig. 8, since the relative increase of K_R/K_0 at $\Delta a/R_0 = 5.5$ is larger. It is noted that here the steady-state toughness, $K^{ss}/K_0 = 3.09$, has been reached for $T = 0$, while the toughness still increases strongly for $T/\sigma_Y = -1$. It is also noted that the initial slope is a great deal higher for the negative T-stress.

In Fig. 10 the debonding peak stress is kept equal to that in Fig. 8, $\hat{\sigma}_0/\sigma_Y = 4.0$, but the critical strain value is increased to $\varepsilon_c = 0.05$. Thus, here the curve for $T = 0$ is that for $\varepsilon_c = 0.05$ in Fig. 7. It is seen that in this case the difference between the two resistance curves at $\Delta a/R_0 = 5.5$ is similar to that found in Fig. 8, but at a higher level of K_R/K_0, so

that the relative difference is actually smaller. Also here the initial slope of the resistance curve is clearly higher for the negative T-stress.

4. CONCLUDING DISCUSSION

Initiation toughness in metals whose mechanism of fracture is void growth and coalescence is proportional to the product of yield stress and void spacing, $\Gamma_0 \simeq \sigma_Y D$, as originally detailed by Rice and Johnson (1970) and as seen in the present model. The initial area fraction of the voids on the fracture plane, f_0, is an independent parameter, which largely controls the crack growth resistance when there is no void nucleation, as documented in the Introduction. In particular, the relation (1) for the enhancement of the steady-state toughness above the initiation toughness can be expressed again as $\Gamma_{ss}/\Gamma_0 = F(f_0, N)$, which is plotted in Fig. 3.

In this paper a modification of the traction–separation law on which the results of Fig. 3 are based has been considered for the purpose of examining the role of the intense plastic strain in the immediate vicinity of the crack tip on accelerating the void growth process and on nucleating more voids. The modification reduces the peak separation stress $\hat{\sigma}$ continuously as a function of local plastic strain for plastic strains above a critical value ε_c. The modification has essentially no influence on the initiation toughness characterizing the onset of crack growth (recall that the normalizing factor K_0 in Figs 5–10 is defined in (6) and (8) in terms of the initial peak traction stress, $\hat{\sigma}_0$). Moreover, when ε_c is larger than about a value between 0.05 and 0.1, depending somewhat on $\hat{\sigma}_0$, N and δ_c/Δ_0, the modification also has little influence on crack growth resistance, since the full crack growth resistance of the unmodified model then develops. However, when ε_c is less than this value, significant reductions in the crack growth resistance take place. Quantitative connections between the trends predicted by the modification and the micromechanics of void nucleation and growth cannot be made, but qualitative implications can be drawn.

In the regime of multiple void interaction, crack growth tearing resistance, as opposed to initiation, depends primarily on the void volume fraction on the potential fracture plane. Increasing this void volume fraction by the nucleation of additional voids, perhaps associated with a population of smaller second phase particles, has the potential of significantly lowering the *relative* crack growth resistance (e.g. Γ_{ss}/Γ_0) if the plastic strain at which they are nucleated is not too large. This is the type of behaviour represented by the present plastic strain dependent traction–separation law. Conversely, control of the distribution of void-nucleating particles in such a way as to reduce the effective value of f_0 on the path of least resistance in front of the crack tip will increase the crack growth resistance without necessarily increasing the initiation toughness, which is tied more closely to the spacing D of the primary voids. The results in Fig. 3 suggest that relatively small changes in f_0 can have relatively large effects on the crack growth resistance, further emphasizing the importance of control of the population of voids. In the regime of void by void growth, the traction law modification employed here predicts crack growth even at high levels of $\hat{\sigma}_0/\sigma_Y$, for which the model without modification would only result in crack tip blunting.

In the regime of void by void growth a model such as the present one, based on an embedded cohesive zone, does not directly account for the interaction of the crack tip and the voids nearest to it and therefore the interaction can only be represented qualitatively. Alternative computational models are those based on a porous ductile material model, as applied by Needleman and Tvergaard (1987, 1991), Rousselier (1987), Sun *et al.* (1992), Brocks *et al.* (1994) and Xia *et al.* (1995). In these finite element models the mesh must capture the interaction between the tip and the near-tip voids on the order of a distance D away as the tip advances, and void spacing D needs to enter explicitly in the models. A highly refined fine scale analysis of the tip–void interaction is currently out of reach with such models. Instead, nearly all these models have taken the element size to be on the order of D, and some models have used the interpretation that void containing elements are situated along the plane ahead of the crack tip. As such, these models display mesh dependence. To be used effectively, a particular mesh choice for a given material must be

calibrated against at least one set of experimental crack growth data. This procedure is discussed in some detail by Xia *et al.* (1995). The present model also displays mesh dependence in its modified form, since the plastic strain near the tip is sensitive to the size of the finite elements along the line of the crack. When this model based on the embedded cohesive zone is used for a particular material, both the parameter values specifying the traction–separation law and the mesh size along the crack growth path must be kept fixed.

Acknowledgements—The work of J.W.H. was supported in part by the National Science Foundation (grant no. MSS-92-02141) and by the Division of Applied Sciences, Harvard University.

REFERENCES

Brocks, W., Klingbeil, Kunecke, D. and Sun, D.-Z. (1994). Application of the Gurson model to ductile tearing resistance. In *Constraint Effects in Fracture: Theory and Applications, ASTM STP* **1244** (Edited by M. Kirk and A. Bakker). American Society for Testing and Materials, Philadelphia. In press.

Gurson, A. L. (1977). Continuum theory of ductile rupture by void nucleation and growth: Part I—yield criteria and flow rules for porous ductile media. *J. Engng Mater. Tech.* **99,** 2–15.

Hutchinson, J. W. (1973). Finite strain analysis of elastic–plastic solids and structures. In *Numerical Solution of Nonlinear Structural Problems* (Edited by R. F. Hartung), p. 17. American Society for Mechanical Engineers, New York.

Needleman, A. and Tvergaard, V. (1987). An analysis of ductile rupture modes at a crack tip. *J. Mech. Phys. Solids* **35,** 151–183.

Needleman, A. and Tvergaard, V. (1991). An analysis of dynamic, ductile crack growth in a double edge cracked specimen. *Int. J. Fracture* **49,** 41–67.

Paris, P. C., Tada, H., Zahoor, A. and Ernst, H. (1979). The theory of instability of the tearing mode of elastic–plastic crack growth. In *Elastic–Plastic Fracture* (Edited by J. D. Landes *et al.*), pp. 5–36. ASTM STP 668, American Society of Testing Materials.

Rice, J. R. and Johnson, M. A. (1970). The role of large crack tip geometry changes in plane strain fracture. In *Inelastic Behaviour of Solids* (Edited by M. F. Kanninen *et al.*), pp. 641–672. McGraw–Hill, New York.

Rousselier, G. (1987). Ductile fracture models and their potential in local approach of fracture. *Nucl. Engng Des.* **105,** 97–111.

Sun, D.-Z., Kienzler, R., Voss, B. and Schmitt, W. (1992). Application of micromechanical models to the prediction of ductile fracture. In *Fracture Mechanics: Twenty-Second Symposium (Volume II), ASTM STP* **1131** (Edited by S. N. Atluri, J. C. Newman, Jr, I. S. Raju and J. S. Epstein), pp. 368–378. American Society for Testing and Materials, Philadelphia.

Tvergaard, V. (1990a). Material failure by void growth to coalescence. *Adv. app. Mech.* **27,** 83–151.

Tvergaard, V. (1990b). Effect of fibre debonding in a whisker-reinforced metal. *Mater. Sci. Engng* **A125,** 203–213.

Tvergaard, V. (1992). Effect of ductile particle debonding during crack bridging in ceramics. *Int. J. Mech. Sci.* **34,** 635–649.

Tvergaard, V. (1994). Cavity growth in ductile particles bridging a brittle matrix crack. Report no. 491, Danish Center for Applied Mathematics and Mechanics.

Tvergaard, V. and Hutchinson, J. W. (1992). The relation between crack growth resistance and fracture process parameters in elastic–plastic solids. *J. Mech. Phys. Solids* **40,** 1377–1397.

Tvergaard, V. and Hutchinson, J. W. (1994). Effect of *T*-stress on mode I crack growth resistance in a ductile solid. *Int. J. Solids Struct.* **31,** 823–833.

Xia, L., Shih, C. F. and Hutchinson, J. W. (1995). A computational approach to ductile crack growth under large scale yielding conditions. *J. Mech. Phys. Solids.* **43,** 389–430.